Two-Dimensional DOA Estimation Using Two Parallel Nested Arrays

Zhi Zheng and Shilin Mu

***Abstract*— In this letter, we propose a new method for two-dimensional (2-D) direction-of-arrival (DOA) estimation using two parallel nested arrays. In this method, an augmented covariance matrix is firstly constructed using the outputs of two parallel difference coarrays. Based on the augmented covariance matrix, the 2-D DOA estimation problem is then converted into two one-dimensional estimation problems. Finally, the azimuth and elevation angle estimates are derived using the estimated direction cosines. Unlike the traditional methods, our algorithm exploits the difference coarray to increase the array aperture and degrees of freedom. Moreover, it does not require any peak searching and can achieve parameter automatic pairing. Numerical simulations are conducted to verify the performance of the proposed method.**

***Index Terms*— DOA estimation, two-parallel nested array (TPNA), degrees of freedom (DOFs), array aperture.**

I. Introduction

DIRECTION-OF-ARRIVAL (DOA) estimation is known to be a fundamental problem in many fields such as wireless communications, radar and sonar. In practice, it is more significant to estimate the two-dimensional (2-D) DOAs (i.e., azimuth and elevation angles) of signals. Compared with one-dimensional (1-D) DOA estimation, the studies on 2-D DOA estimation pay particular attention to alleviating the computational burden and handling parameter pairing, which are critical for practical application. Many 2-D DOA estimation methods employing multiple uniform linear arrays (ULAs) have been suggested in the past decades. They can be roughly classified based on array geometry, into the following categories: the rectangular array [1]–[3], the L-shaped array [4]–[8] and the two-parallel-shaped array [9]–[11].

Recently, nested arrays have aroused wide attention owing to their advantages in array aperture and degrees of freedom (DOFs) over conventional ULAs. For a two-level nested array, we can achieve $2M_2(M_1+1)-1$ DOFs in the coarray using only M_1+M_2 sensors [12]. Furthermore, it can guarantee a hole-free difference coarray. These excellent properties leads to many DOA estimation techniques using nested arrays [13]–[18]. Nevertheless, most of them only consider the problem of 1-D DOA estimation.

Manuscript received November 13, 2019; revised December 3, 2019 and December 6, 2019; accepted December 7, 2019. Date of publication December 10, 2019; date of current version March 10, 2020. This work was supported in part by the Sichuan Science and Technology Program under Grant 2019YJ0191, and by the Fundamental Research Funds for the Central Universities of China under Grant 2672018ZYGX2018J003. The associate editor coordinating the review of this letter and approving it for publication was S. Majhi. *(Corresponding author: Zhi Zheng.)*

The authors are with the School of Information and Communication Engineering, University of Electronic Science and Technology of China, Chengdu 611731, China (e-mail: zz@uestc.edu.cn; mushilin_china@163.com).

Digital Object Identifier 10.1109/LCOMM.2019.2958903

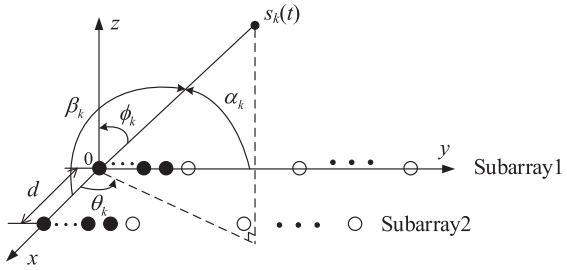

Fig. 1. Two-parallel nested array configuration.

In this letter, an algorithm for 2-D angle estimation with two parallel nested arrays is suggested. Unlike the traditional methods, our algorithm derives the DOA estimates based on an augmented covariance matrix that is constructed using the output signals of two parallel difference coarrays. That is equivalent to increasing the array aperture and achievable DOFs. Therefore, our algorithm can offer higher estimation accuracy and deal with more sources than the traditional approaches. Additionally, it does not involve peak searching and parameter pairing process. Simulation results demonstrate the superiority of the proposed algorithm over the existing approaches.

Notations: $(\cdot)^*$, $(\cdot)^T$ and $(\cdot)^H$ represent the complex conjugate, transpose and conjugate transpose operators, respectively. $E\{\cdot\}$ is the statistical expectation, $\mathrm{vec}(\cdot)$ denotes the vectorization operator, and $\|\cdot\|_F$ means the Frobenius norm. $\mathrm{diag}(\mathbf{a})$ means a diagonal matrix whose diagonal elements are the elements of $\mathbf{a}$. $\arg(\cdot)$ stands for the argument of a complex number. $\mathbf{I}_M$ denotes the $M\times M$ identity matrix, and $\mathbf{0}_{\bar{M}\times 1}$ means the $\bar{M}\times 1$ all-zero vector. $[\cdot]_m$ is the mth element of a vector. The symbol $\otimes$ denotes the Kronecker product.

II. Array Data Model

We consider a two-parallel nested array (TPNA) located at the x-y plane as displayed in Fig. 1. The array is formed by two parallel subarrays with a displacement of $d=\lambda/2$, where λ denotes the carrier wavelength. Each subarray is a two-level nested array consisting of M sensors. The inner ULA contains M_1 sensors with spacing d_1, and the outer ULA contains M_2 sensors with spacing $d_2=(M_1+1)d_1$. For subarray 1, the sensor positions are $(0, z_i d_1)$, where z_i belongs to an integer set $\mathbb{S} \triangleq \{z_i, i=1,2,\ldots,M\} = \{0,1,\ldots,M_1-1,M_1,2(M_1+1)-1,\ldots,M_2(M_1+1)-1\}$. For subarray 2, the sensor positions are denoted by $(d, z_i d_1)$.

Assume K narrowband uncorrelated signals impinge on the array from 2-D distinct directions $\{(\theta_k,\phi_k)\}_{k=1}^K$, where θ_k and ϕ_k denote the azimuth and elevation angles of the kth signal, respectively. Furthermore, the incident directions can be represented by $\{(\alpha_k,\beta_k)\}_{k=1}^K$, as depicted in Fig. 1.

The measurements at subarrays 1 and 2 are given by

$$\mathbf{x}_1(t) = \mathbf{A}_1\mathbf{s}(t) + \mathbf{n}_1(t) \quad (1)$$

$$\mathbf{x}_2(t) = \mathbf{A}_2\mathbf{s}(t) + \mathbf{n}_2(t) \quad (2)$$

where $\mathbf{s}(t) = [s_1(t), s_2(t), \cdots, s_K(t)]^T$ denotes the signal waveform vector, $\mathbf{n}_1(t)$ and $\mathbf{n}_2(t)$ are the additive white Gaussian noise vectors, and uncorrelated with the source signals, $\mathbf{A}_1 = [\mathbf{a}_1(\alpha_1), \ldots, \mathbf{a}_1(\alpha_K)]$ is the manifold matrix of subarray 1, where $\mathbf{a}_1(\alpha_k) = [1, e^{j2\pi z_2 d_1 \cos(\alpha_k)/\lambda}, \ldots, e^{j2\pi z_M d_1 \cos(\alpha_k)/\lambda}]^T$ is the array manifold associated with the kth signal with $\cos(\alpha_k) = \sin(\theta_k)\sin(\phi_k)$, $\mathbf{A}_2 = [\mathbf{a}_2(\alpha_1, \beta_1), \ldots, \mathbf{a}_2(\alpha_K, \beta_K)] = \mathbf{A}_1\mathbf{\Phi}$ is the manifold matrix of subarray 2 with $\mathbf{\Phi} = \mathrm{diag}(e^{j2\pi d \cos(\beta_1)/\lambda}, \ldots, e^{j2\pi d \cos(\beta_K)/\lambda})$ and $\cos(\beta_k) = \cos(\theta_k)\sin(\phi_k)$.

III. Proposed Algorithm

The covariance matrix of $\mathbf{x}_1(k)$ is defined as

$$\mathbf{R}_{11} \triangleq E\{\mathbf{x}_1(k)\mathbf{x}_1^H(k)\} = \mathbf{A}_1\mathbf{\Lambda}\mathbf{A}_1^H + \sigma_n^2\mathbf{I}_M \quad (3)$$

where $\mathbf{\Lambda} = E\{\mathbf{s}(t)\mathbf{s}^H(t)\} = \mathrm{diag}([\sigma_1^2, \ldots, \sigma_K^2])$ denotes the signal covariance matrix, and σ_n^2 is the noise variance.

Vectorizing $\mathbf{R}_{11}$ yields

$$\mathbf{z}_1 = \mathrm{vec}(\mathbf{R}_{11}) = \mathbf{B}_1\mathbf{p} + \sigma_n^2\vec{\mathbf{1}}_n \quad (4)$$

where $\mathbf{B}_1 = [\mathbf{a}_1^*(\alpha_1) \otimes \mathbf{a}_1(\alpha_1), \ldots, \mathbf{a}_1^*(\alpha_K) \otimes \mathbf{a}_1(\alpha_K)]$, $\mathbf{p} = [\sigma_1^2, \sigma_2^2, \ldots, \sigma_K^2]^T$, and $\vec{\mathbf{1}}_n = [\mathbf{e}_1^T, \mathbf{e}_2^T, \ldots, \mathbf{e}_M^T]^T$ with $\mathbf{e}_i$ being a column vector of all zeros except one 1 at the ith position.

Removing the redundant rows from $\mathbf{z}_1$ and rearranging them to give

$$\bar{\mathbf{z}}_1 = \bar{\mathbf{B}}_1\mathbf{p} + \sigma_n^2\vec{\mathbf{e}}' \quad (5)$$

where $\bar{\mathbf{B}}_1 \in \mathbb{C}^{(2M_2(M_1+1)-1)\times K}$ is a manifold matrix, and $\vec{\mathbf{e}}' \in \mathbb{C}^{(2M_2(M_1+1)-1)\times 1}$ denotes an all-zero vector except one 1 at the $M_2(M_1+1)$th location.

From the vector $\bar{\mathbf{z}}_1$, we construct the Toeplitz matrix [19]:

$$\tilde{\mathbf{R}}_{11} = \begin{bmatrix} [\bar{\mathbf{z}}_1]_{\bar{M}} & [\bar{\mathbf{z}}_1]_{\bar{M}-1} & \cdots & [\bar{\mathbf{z}}_1]_1 \\ [\bar{\mathbf{z}}_1]_{\bar{M}+1} & [\bar{\mathbf{z}}_1]_{\bar{M}} & \cdots & [\bar{\mathbf{z}}_1]_2 \\ \vdots & \vdots & \ddots & \vdots \\ [\bar{\mathbf{z}}_1]_{2\bar{M}-1} & [\bar{\mathbf{z}}_1]_{2\bar{M}-2} & \cdots & [\bar{\mathbf{z}}_1]_{\bar{M}} \end{bmatrix} \quad (6)$$

where $\bar{M} = M_2(M_1+1)$.

The cross-covariance matrix between $\mathbf{x}_2(t)$ and $\mathbf{x}_1(t)$ is:

$$\mathbf{R}_{21} \triangleq E\{\mathbf{x}_2(t)\mathbf{x}_1^H(t)\} = \mathbf{A}_2\mathbf{\Lambda}\mathbf{A}_1^H. \quad (7)$$

Vectorizing $\mathbf{R}_{21}$ yields the noise-free vector:

$$\mathbf{z}_2 = \mathrm{vec}(\mathbf{R}_{21}) = \mathbf{B}_2\mathbf{p}. \quad (8)$$

where $\mathbf{B}_2 = [\mathbf{a}_1^*(\alpha_1) \otimes \mathbf{a}_2(\alpha_1, \beta_1), \ldots, \mathbf{a}_1^*(\alpha_K) \otimes \mathbf{a}_2(\alpha_K, \beta_K)]$, and we can easily derive $\mathbf{B}_2 = \mathbf{B}_1\mathbf{\Phi}$.

Removing the redundant rows from $\mathbf{z}_2$ and rearranging them to form

$$\bar{\mathbf{z}}_2 = \bar{\mathbf{B}}_2\mathbf{p}. \quad (9)$$

where $\bar{\mathbf{B}}_2 \in \mathbb{C}^{(2\bar{M}-1)\times K}$ is a manifold matrix, and the relation $\bar{\mathbf{B}}_2 = \bar{\mathbf{B}}_1\mathbf{\Phi}$ holds.

From the vector $\bar{\mathbf{z}}_2$, we form the Toeplitz matrix:

$$\tilde{\mathbf{R}}_{21} = \begin{bmatrix} [\bar{\mathbf{z}}_2]_{\bar{M}} & [\bar{\mathbf{z}}_2]_{\bar{M}-1} & \cdots & [\bar{\mathbf{z}}_2]_1 \\ [\bar{\mathbf{z}}_2]_{\bar{M}+1} & [\bar{\mathbf{z}}_2]_{\bar{M}} & \cdots & [\bar{\mathbf{z}}_2]_2 \\ \vdots & \vdots & \ddots & \vdots \\ [\bar{\mathbf{z}}_2]_{2\bar{M}-1} & [\bar{\mathbf{z}}_2]_{2\bar{M}-2} & \cdots & [\bar{\mathbf{z}}_2]_{\bar{M}} \end{bmatrix}. \quad (10)$$

The matrix $\tilde{\mathbf{R}}_{11}$ can be expressed as [12], [19]:

$$\tilde{\mathbf{R}}_{11} = \bar{\mathbf{B}}_{11}\mathbf{\Lambda}\bar{\mathbf{B}}_{11}^H + \sigma_n^2\mathbf{I}_{\bar{M}}. \quad (11)$$

where $\bar{\mathbf{B}}_{11} = [\mathbf{b}_1(\alpha_1), \ldots, \mathbf{b}_1(\alpha_K)] \in \mathbb{C}^{\bar{M}\times K}$ consists of the last $\bar{M}$ rows of $\bar{\mathbf{B}}_1$.

Similarly, the matrix $\tilde{\mathbf{R}}_{21}$ can be expressed as

$$\tilde{\mathbf{R}}_{21} = \bar{\mathbf{B}}_{21}\mathbf{\Lambda}\bar{\mathbf{B}}_{11}^H. \quad (12)$$

where $\bar{\mathbf{B}}_{21} = [\mathbf{b}_2(\alpha_1, \beta_1), \ldots, \mathbf{b}_2(\alpha_K, \beta_K)] \in \mathbb{C}^{\bar{M}\times K}$ consists of the last $\bar{M}$ rows of $\bar{\mathbf{B}}_2$, and $\bar{\mathbf{B}}_{21} = \bar{\mathbf{B}}_{11}\mathbf{\Phi}$.

Now, we form an $2\bar{M} \times 2\bar{M}$ matrix as

$$\tilde{\mathbf{R}} = \begin{bmatrix} \tilde{\mathbf{R}}_{11} & \tilde{\mathbf{R}}_{21}^H \\ \tilde{\mathbf{R}}_{21} & \tilde{\mathbf{R}}_{11} \end{bmatrix} = \bar{\mathbf{B}}\mathbf{\Lambda}\bar{\mathbf{B}}^H + \sigma_n^2\mathbf{I}_{2\bar{M}}. \quad (13)$$

where $\bar{\mathbf{B}} = [\bar{\mathbf{B}}_{11}^T, \bar{\mathbf{B}}_{21}^T]^T = [\bar{\mathbf{b}}(\alpha_1, \beta_1), \ldots, \bar{\mathbf{b}}(\alpha_K, \beta_K)]$ behaves like the manifold matrix of two longer parallel ULAs, termed two-parallel difference coarray (TPDC), with

$$\begin{aligned} \bar{\mathbf{b}}(\alpha, \beta) &= \begin{bmatrix} \mathbf{b}_1(\alpha) \\ \mathbf{b}_2(\alpha, \beta) \end{bmatrix} = \begin{bmatrix} \mathbf{b}_1(\alpha) \\ \mathbf{b}_1(\alpha)e^{j2\pi d \cos(\beta)/\lambda} \end{bmatrix} \\ &= \begin{bmatrix} \mathbf{b}_1(\alpha) & \mathbf{0}_{\bar{M}\times 1} \\ \mathbf{0}_{\bar{M}\times 1} & \mathbf{b}_1(\alpha) \end{bmatrix} \begin{bmatrix} 1 \\ e^{j2\pi d \cos(\beta)/\lambda} \end{bmatrix}. \end{aligned} \quad (14)$$

To estimate the 2-D angles, we may create the spectral function:

$$f(\alpha, \beta) = \bar{\mathbf{b}}^H(\alpha, \beta)\mathbf{E}_n\mathbf{E}_n^H\bar{\mathbf{b}}(\alpha, \beta). \quad (15)$$

where $\mathbf{E}_n \in \mathbb{C}^{2\bar{M}\times(2\bar{M}-K)}$ is composed of the eigenvectors of $\tilde{\mathbf{R}}$ corresponding to the $(2\bar{M} - K)$ smallest eigenvalues. However, the 2-D searching is computationally expensive, and it can be replaced by polynomial root-finding.

The matrix $\mathbf{E}_n$ can be partitioned as

$$\mathbf{E}_n = \begin{bmatrix} \mathbf{E}_{n1} \\ \mathbf{E}_{n2} \end{bmatrix} \quad (16)$$

where $\mathbf{E}_{n1}$ and $\mathbf{E}_{n2}$ are size of $\bar{M} \times (2\bar{M} - K)$.

Then, (15) becomes

$$f(\alpha, \beta) = \boldsymbol{\xi}^H\mathbf{Q}(\alpha)\boldsymbol{\xi} \quad (17)$$

where

$$\boldsymbol{\xi} = \begin{bmatrix} 1 \\ e^{j2\pi d \cos(\beta)/\lambda} \end{bmatrix} \quad (18)$$

$$\mathbf{Q}(\alpha) = \begin{bmatrix} \mathbf{b}_1^H(\alpha)\mathbf{E}_{n1}\mathbf{E}_{n1}^H\mathbf{b}_1(\alpha) & \mathbf{b}_1^H(\alpha)\mathbf{E}_{n1}\mathbf{E}_{n2}^H\mathbf{b}_1(\alpha) \\ \mathbf{b}_1^H(\alpha)\mathbf{E}_{n2}\mathbf{E}_{n1}^H\mathbf{b}_1(\alpha) & \mathbf{b}_1^H(\alpha)\mathbf{E}_{n2}\mathbf{E}_{n2}^H\mathbf{b}_1(\alpha) \end{bmatrix}. \quad (19)$$

Note that in (17), the angles α and β are contained in $\mathbf{Q}(\alpha)$ and $\boldsymbol{\xi}$, respectively.

Let $v = \exp[j2\pi d_1 \cos(\alpha)/\lambda]$, we can write $\mathbf{b}_1(\alpha)$ as $\mathbf{b}_1(v) = [1, v, v^2, \ldots, v^{\bar{M}-1}]^T$. Then, the matrix $\mathbf{Q}(\alpha)$ can be characterized by v. The angles $\{\alpha_k\}_{k=1}^K$ can be obtained by finding the roots of the polynomial of v:

$$\det\{\mathbf{Q}(v)\} = p_1p_4 - p_2p_3 = 0 \quad (20)$$

where

$$p_1 = \mathbf{b}_1^H(v)\mathbf{E}_{n1}\mathbf{E}_{n1}^H\mathbf{b}_1(v), \quad (21)$$

$$p_2 = \mathbf{b}_1^H(v)\mathbf{E}_{n1}\mathbf{E}_{n2}^H\mathbf{b}_1(v), \quad (22)$$

$$p_3 = \mathbf{b}_1^H(v)\mathbf{E}_{n2}\mathbf{E}_{n1}^H\mathbf{b}_1(v), \quad (23)$$

$$p_4 = \mathbf{b}_1^H(v)\mathbf{E}_{n2}\mathbf{E}_{n2}^H\mathbf{b}_1(v). \quad (24)$$

Equation (20) can be efficiently solved by using the polynomial root-finding algorithm [20]. The direction cosines $\{\cos(\alpha_k)\}_{k=1}^K$ are estimated as

$$\cos(\hat{\alpha}_k) = \frac{\arg(v_k)}{2\pi d_1/\lambda}, \quad k = 1, \cdots, K. \quad (25)$$

where v_k is one of the roots chosen for $\hat{\alpha}_k$.

Substituting $\cos(\hat{\alpha}_k)$ into (19) yields $\mathbf{Q}(\hat{\alpha}_k)$. The eigenvector corresponding to the minimum eigenvalue of $\mathbf{Q}(\hat{\alpha}_k)$ is

$$\boldsymbol{\xi} = \begin{bmatrix} 1 \\ -\frac{\mathbf{b}_1^H(\hat{\alpha}_k)\mathbf{E}_{n2}\mathbf{E}_{n1}^H\mathbf{b}_1(\hat{\alpha}_k)}{\mathbf{b}_1^H(\hat{\alpha}_k)\mathbf{E}_{n1}\mathbf{E}_{n1}^H\mathbf{b}_1(\hat{\alpha}_k)} \end{bmatrix}. \quad (26)$$

Comparing (18) and (26) results in

$$\cos(\hat{\beta}_k) = \frac{\arg(-\mathbf{b}_1^H(\hat{\alpha}_k)\mathbf{E}_{n2}\mathbf{E}_{n1}^H\mathbf{b}_1(\hat{\alpha}_k))}{2\pi d/\lambda}, \quad k = 1, \cdots, K. \quad (27)$$

With the estimates $\{\cos(\hat{\alpha}_k)\}_{k=1}^K$ and $\{\cos(\hat{\beta}_k)\}_{k=1}^K$, the 2-D angles of the incident signals are calculated by

$$\hat{\theta}_k = \tan^{-1}\left[\frac{\cos(\hat{\alpha}_k)}{\cos(\hat{\beta}_k)}\right], \quad k = 1, \cdots, K, \quad (28)$$

$$\hat{\phi}_k = \sin^{-1}\left[\sqrt{\cos^2(\hat{\alpha}_k)+\cos^2(\hat{\beta}_k)}\right], \quad k=1, \cdots, K. \quad (29)$$

IV. Discussion

A. DOFs and Array Aperture

The proposed method can estimate $2(\bar{M}-1)$ signals at most using a TPNA of $2M$ sensors. In contrast, the 2-D MUSIC method can resolve up to $2M-1$ signals using a two-parallel ULA (TPULA) of $2M$ sensors, and the decoupled algorithm [9] can identify up to $2(M-1)$ signals, while the DOFs of the improved PM method [10] is only $M-1$. On the other hand, the proposed method achieves an array aperture of $(\bar{M}-1)d_1$, while the other three utilize the same array aperture, $(M-1)d_1$.

B. Computational Complexity

For the proposed method, the major calculations involved are to estimate $\mathbf{R}_{11}$ and $\mathbf{R}_{21}$, to perform eigenvalue decomposition on $\tilde{\mathbf{R}}$. The resulting number of flops is roughly $\mathcal{O}\{2M^2N + (2\bar{M})^3\}$, where N is the number of snapshots and in general $N \gg M$. By contrast, the number of flops required by the 2-D MUSIC method is about $\mathcal{O}\{(2M)^2N + (2M)^2G_1G_2 + (2M)^3\}$, where G_1 and G_2 regulate a fine 2-D grid with $G_1, G_2 \gg M$. The decoupled algorithm [9] takes about $\mathcal{O}\{(2M)^2N+(2M)^3\}$ calculation flops. While the improved PM method [10] only requires roughly $\mathcal{O}\{(2M+1)^2(N+K)+3K^3+(8M-1)K^2+(4M-1)K\}$ calculation flops. Consequently, our approach has lower complexity than the 2-D MUSIC method, but it is computationally more intensive than the remaining methods.

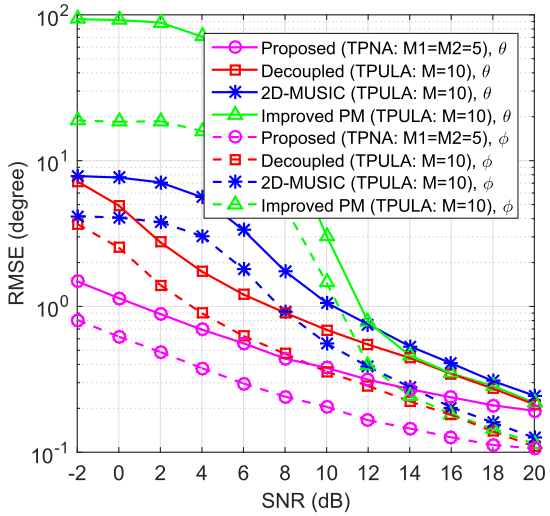

Fig. 2. RMSEs of azimuth and elevation angle estimates versus SNR.

V. Simulation Examples

Simulation examples are presented to illustrate the performance of the proposed method in comparison with the 2-D MUSIC method, the decoupled method [9] and the improved PM method [10]. In all examples, we consider a TPNA with $M_1 = M_2 = 5$ and $d_1 = \lambda/2$ for the proposed method, a TPULA with $M = 10$ and sensor spacing $\lambda/2$ is used for the compared methods. Moreover, a search interval of 0.1° is adopted for the 2-D MUSIC method. The simulation results are evaluated by the root-mean-square error (RMSE) from the average of 1000 independent trials.

A. Example 1—RMSE Versus SNR

Two uncorrelated signals arrive at the array from 2-D directions $(-60^\circ, 30^\circ)$ and $(-40^\circ, 40^\circ)$. The SNR is varied from -2 dB to 20 dB, while the number of snapshots is set to $N = 500$. The RMSEs of azimuth and elevation angle estimates versus SNR are displayed in Fig. 2. It can be observed that for azimuth and elevation angle estimation, the proposed approach evidently outperforms the other methods across a wide range of SNR. Especially, the RMSEs of the proposed method are close to 1° when the SNR is -2 dB. That is because the proposed approach exploits the virtual aperture of the TPNA compared to its rivals.

B. Example 2—RMSE Versus Number of Snapshots

The number of snapshots is varied from 100 to 1000, and the SNR is fixed at 15 dB, while the angular parameters are the same as those in the first example. The RMSEs of azimuth and elevation angle estimates against the number of snapshots are plotted in Fig. 3. It is clearly seen that the numerical results are consistent with those in the first example. As the number of snapshots increases, the corresponding RMSE becomes smaller for each algorithm, but our approach

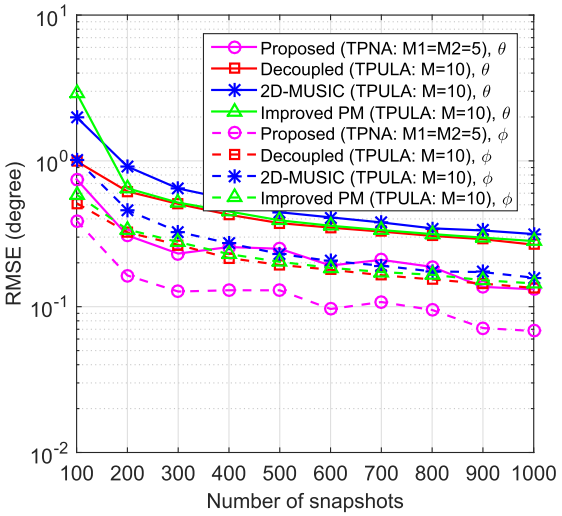

Fig. 3. RMSEs of azimuth and elevation angle estimates versus the number of snapshots.

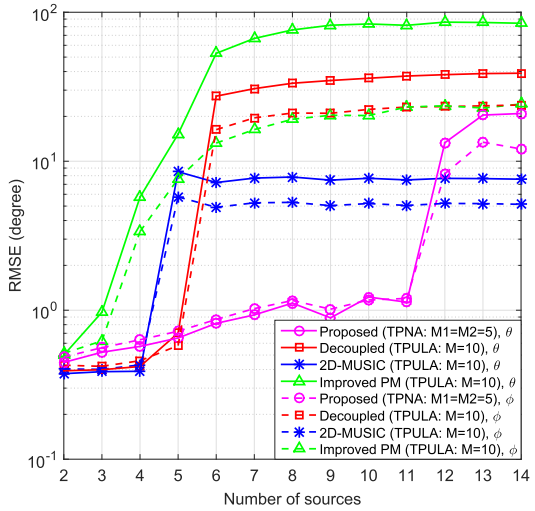

Fig. 4. RMSEs of azimuth and elevation angle estimates versus the number of sources.

offers the minimum RMSE among the algorithms compared here due to the array aperture advantage.

C. Example 3—RMSE Versus Number of Sources

The SNR is equal to 0 dB, while the number of snapshots is set as $N = 200$. The sources are located at $\{(\theta_k,\phi_k)\}_{k=1}^{K}$, where $\theta_k = 20^\circ+45^\circ(k-1)/(K-1)$ and $\phi_k = 30^\circ+30^\circ(k-1)/(K-1)$. The RMSEs of azimuth and elevation angle estimates against the number of sources are depicted in Fig. 4. When K is equal to 2, all the algorithms achieve satisfactory performance and their RMSEs are less than 0.5°. Along with the increase of K, the performance of the improved PM method, the 2-D MUSIC method and the decoupled method will rapidly deteriorate. In comparison, our proposed method exhibits more stable performance that begins to apparently degrade until K exceeds 11, owning to the DOFs superiority.

VI. Conclusion

In this letter, we have presented a 2-D DOA estimator based on the TPNA. Compared with the traditional methods, the proposed estimator utilizes an increased array aperture and an enhanced DOFs by forming an augmented covariance matrix based on the TPDC output signals. Furthermore, it avoids peak searching and extra parameter pairing, and thus brings about a low computational complexity. Simulation results indicate that our approach significantly outperforms the traditional algorithms using the TPULA with the same number of sensors.

References

[1] M. D. Zoltowski, M. Haardt, and C. P. Mathews, "Closed-form 2-D angle estimation with rectangular arrays in element space or beamspace via unitary ESPRIT," *IEEE Trans. Signal Process.*, vol. 44, no. 2, pp. 316–328, Feb. 1996.

[2] P. Strobach, "Two-dimensional equirotational stack subspace fitting with an application to uniform rectangular arrays and ESPRIT," *IEEE Trans. Signal Process.*, vol. 48, no. 7, pp. 1902–1914, Jul. 2000.

[3] X. Fu, R. Cao, and F. Wen, "A de-noising 2-D-DOA estimation method for uniform rectangle array," *IEEE Commun. Lett.*, vol. 22, no. 9, pp. 1854–1857, Sep. 2018.

[4] G. Wang, J. Xin, N. Zheng, and A. Sano, "Computationally efficient subspace-based method for two-dimensional direction estimation with L-shaped array," *IEEE Trans. Signal Process.*, vol. 59, no. 7, pp. 3197–3212, Jul. 2011.

[5] Y.-Y. Dong, C.-X. Dong, J. Xu, and G.-Q. Zhao, "Computationally efficient 2-D DOA estimation for L-shaped array with automatic pairing," *IEEE Antennas Wireless Propag. Lett.*, vol. 15, pp. 1669–1672, 2016.

[6] N. Tayem, K. Majeed, and A. A. Hussain, "Two-dimensional DOA estimation using cross-correlation matrix with L-shaped array," *IEEE Antennas Wireless Propag. Lett.*, vol. 15, pp. 1077–1088, 2016.

[7] Y. Dong, C. Dong, W. Liu, H. Chen, and G. Zhao, "2-D DOA estimation for L-shaped array with array aperture and snapshots extension techniques," *IEEE Signal Process. Lett.*, vol. 24, no. 4, pp. 495–499, Apr. 2017.

[8] J. Li and D. Jiang, "Joint elevation and azimuth angles estimation for L-shaped array," *IEEE Antennas Wireless Propag. Lett.*, vol. 16, pp. 453–456, 2017.

[9] T. Xia, Y. Zheng, Q. Wan, and X. Wang, "Decoupled estimation of 2-D angles of arrival using two parallel uniform linear arrays," *IEEE Trans. Antennas Propag.*, vol. 55, no. 9, pp. 2627–2632, Sep. 2007.

[10] J. Li, X. Zhang, and H. Chen, "Improved two-dimensional DOA estimation algorithm for two-parallel uniform linear arrays using propagator method," *Signal Process.*, vol. 92, no. 12, pp. 3032–3038, Dec. 2012.

[11] Z. Zheng, Y. Yang, W.-Q. Wang, and S. Zhang, "Two-dimensional direction estimation of multiple signals using two parallel sparse linear arrays," *Signal Process.*, vol. 143, pp. 112–121, Feb. 2018.

[12] P. Pal and P. P. Vaidyanathan, "Nested arrays: A novel approach to array processing with enhanced degrees of freedom," *IEEE Trans. Signal Process.*, vol. 58, no. 8, pp. 4167–4181, Aug. 2010.

[13] K. Han and A. Nehorai, "Wideband Gaussian source processing using a linear nested array," *IEEE Signal Process. Lett.*, vol. 20, no. 11, pp. 1110–1113, Nov. 2013.

[14] C. Wen, G. Shi, and X. Xie, "Estimation of directions of arrival of multiple distributed sources for nested array," *Signal Process.*, vol. 130, pp. 315–322, Jan. 2017.

[15] Y. Wang, A. Hashemi-Sakhtsari, M. Trinkle, and B. W.-H. Ng, "Sparsity-aware DOA estimation of quasi-stationary signals using nested arrays," *Signal Process.*, vol. 144, pp. 87–98, Mar. 2018.

[16] F. Chen, J. Dai, N. Hu, and Z. Ye, "Sparse Bayesian learning for off-grid DOA estimation with nested arrays," *Digit. Signal Process.*, vol. 82, pp. 187–193, Nov. 2018.

[17] G. Qin, Y. D. Zhang, and M. G. Amin, "DOA estimation exploiting moving dilated nested arrays," *IEEE Signal Process. Lett.*, vol. 26, no. 3, pp. 490–494, Mar. 2019.

[18] Z. Zheng, M. Fu, W. Wang, S. Zhang, and Y. Liao, "Localization of mixed near-field and far-field sources using symmetric double-nested arrays," *IEEE Trans. Antennas Propag.*, vol. 67, no. 11, pp. 7059–7070, Nov. 2019.

[19] C.-L. Liu and P. P. Vaidyanathan, "Remarks on the spatial smoothing step in coarray MUSIC," *IEEE Signal Process. Lett.*, vol. 22, no. 9, pp. 1438–1442, Sep. 2015.

[20] B. D. Rao and K. V. S. Hari, "Performance analysis of root-music," *IEEE Trans. Acoust., Speech, Signal Process.*, vol. 37, no. 12, pp. 1939–1949, Dec. 1989.